Eur Biophys J (1997) 26: 337–348

ARTICLE

L. P. Savtchenko · S. M. Korogod

Spatial electrical patterns in simulated neuronal dendrites

Received: 23 October 1996 / Accepted: 21 May 1997

Abstract Steady state longitudinal distributions of (a) the density of channels conducting an inward transmembrane current of cations, (b) the submembrane concentrations of these cations, and (c) the resting membrane potential, were investigated in a phenomenological model of a cylinder-shaped dendritic process of the neuron. It was found that spatially non-uniform patterns of these distributions occur only if one of the following conditions held (i) an increase in the intracellular concentration of cations conducting an inward passive transmembrane current amplified the active efflux of those cations by the pump and attenuated their passive influx through the voltage dependent channels, with amplification of the efflux lower than attenuation of the influx; (ii) molecules of mobile channels bore a negative electrophoretic charge exposed to the intracellular space and were subject to lateral electrodiffusion in the membrane; (iii) the cations induced a further release of cations from intracellular stores. Numerical simulation studies of the membrane with Na and K channels and Na/K pumps with conditions (i) and (ii) have demonstrated the possibility of the creation of inhomogeneous patterns in the neurites. These inhomogeneous patterns are dissipative structures (*DSs*), and they can be spatially periodic.

Key words Neuron · Membrane · Self-organization · Dissipative structures · Resting membrane potential · Simulation

L. P. Savtchenko (✉)
Research Laboratory of Biophysics and Bioelectronics,
Dniepropetrovsk State University,
72 Gagarin Avenue, 320625 GSP Dniepropetrovsk, Ukraine

S. M. Korogod
Unité de Neurocybernétique Cellulaire,
280 Boulevard Sainte-Marguerite, F-13009 Marseille, France
(Fax: +33 4 91 26 20 38; e-mail: korogod@lnf2.cnrs-mrs.fr)

Introduction

The electrical behavior of neurons is manifested in changes of transmembrane voltages and currents in the soma and the neurites (Rall 1977; Bedlack et al. 1994). These electrical phenomena are defined by spatially distributed electrical conductances of the plasma membrane and the cytoplasm, and by electrochemical potentials of ions carrying transmembrane and core currents. The inhomogeneous distributions of the ion channels, other membrane proteins, and the intracellular concentration of ions, especially Ca^{2+}, are well-known (Chad and Eckert 1984; Hille 1992; Eun-hye Joe and Angelides 1993) but not well-understood. Recently, the spatially inhomogeneous patchy distribution of depolarization was demonstrated using optical methods (Gogan et al. 1995). The authors suggested that these inhomogeneous spatial patterns of depolarization were related to the operation of ionic channels in the membrane.

The aim of this work was to study the possible mechanisms of formation and maintenance of coupled non-uniform steady longitudinal distributions of (i) the density of open channels conducting an inward transmembrane current of cations, (ii) the submembrane concentration of the cations, and (iii) the resting transmembrane potential. We studied a phenomenological model of a neuronal dendrite composed of a membrane cylinder which separated conductive extra- and intracellular media and was equipped with the two kinds of channels conducting passive currents and with one active counter-transport system. This model had the following features. Although it is not clear what proportion of each population of the membrane proteins is mobile (Hille 1992; Peters 1981), one population here (the channels of inward current) was totally mobile, whereas the others (the channels of outward current and the pump molecules) were immobile. Mobile channels bore electrophoretic charge (Cai and Jordan 1990; Becchetti et al. 1992). They were subject to voltage-dependent conformation transitions between open and closed states (Hille 1992) and to lateral electrodiffusion in the membrane (Jaffe 1977; Ryan et al. 1988; Cukierman 1991). Ions moved across the

membrane passively, through open channels and actively, being driven by the pumps. This led to local changes in submembrane ion concentration. The latter was also changed as the result of axial diffusion in a thin submembrane layer (Qian and Sejnowski 1989) and owing to radial fluxes of ion exchange with deeper layers of cytoplasm or the stores (Henzi and MacDermott 1992).

We put forward the hypothesis that these inhomogeneous steady distributions of channels, ions, and voltages are dissipative structures (*DSs*) resulting from diffusion driven instability which are similar to well-known phenomena in other non-linear systems far from thermodynamic equilibrium (Nicolis and Prigogine 1977). The necessary and sufficient conditions for the instability were derived, and then the necessary conditions for those were derived and biologically interpreted.

Theory

1 Glossary

d – diameter of cylinder-shaped cell (μm).
l – length of cylinder-shaped cell (μm).
z, r – longitudinal and radial coordinate, respectively (μm).
t – time (*ms*).
C_m – specific membrane capacitance (μF/cm^2).
D_e – lateral diffusivity of *X*-channels (μm^2/ms).
D_X – diffusivity of *X*-cations (μm^2/ms).
e – density of *X*-channels in both conformational states per unit length of membrane cylinder (μm^{-1}).
σ_X – conductance of a single *X*-channel (pS).
G_Y – membrane conductivity in relation to the current of *Y*-cations (mS/cm^2).
G_L – membrane conductivity in relation to the leak current (mS/cm^2).
F – Faraday's constant (98 C/mmol).
R – gas constant (8.3 (mV C)/mmol °K)).
T – absolute temperature (300 °K).
$\beta = RT/F$ – dimension scaling factor for potentials ($\approx$25 mV).
$J_p(\psi, [X]_i)$ – active (pump) current density (μA/β cm^2).
$J_X(\psi, \rho, [X]_i)$ – density of the passive current of *X*-cations through open *X*-channels (μA/β cm^2).
$J_L(\psi)$ – the leak current density (μA/β cm^2).
$J_Y(\psi)$ – density of the passive current of *Y*-cations (μA/β cm^2).
$[Y]_i$, $[Y]_o$ – intra- and extracellular concentration of *Y*-cations ($[Y]_i > [Y]_o$) (mM).
N_e – electrophoretic charge of a single *X*-channel measured in elementary charges (dimensionless).
P – the parameter that converts concentration to the membrane potential (mM^{-1}).
P_X – rate constant of *X*-cation exchange between the submembrane and deeper layers of the cytoplasm (ms^{-1}).
R_{in} – specific resistivity of cytoplasm (Ohm cm).
$[X]_i$, $[X]_o$ – intra- and extracellular concentration of *X*-cations ($[X]_i < [X]_o$) (mM).
ψ – transmembrane potential (β).
ψ_L – equilibrium potential for the leak current (β).
Λ – conductivity of the ion pump system (mS/cm^2).
χ – effective thickness of the submembrane layer of electrolyte (μm).
ρ – density of open *X*-channels per unit length of the cylinder (μm^{-1}).

2 The model

A cylinder-shaped cell with sealed ends and resistive-capacitive membrane separating intra- and extracellular electrolytes was considered with the following assumptions. Currents across the ion-selective membrane were carried by cations of two sorts, *X* and *Y*, both passively and actively. Passive currents (inward *X* and outward *Y*) passed in the direction of the corresponding electrochemical gradients. Active transport of the cations was driven by the ion pump against the gradient at the expense of chemical energy (Kotyk et al. 1988). *X*-cations crossed the membrane through open *X*-channels. Voltage dependent conformational transitions of *X*-channels changed their state from closed to open and vice versa. *Y*-cations crossed the membrane through open *Y*-channels. The latter were distributed homogeneously along the cell and provided a uniform *Y*-conductivity of the membrane. Active transport of *X* and *Y* cations was considered as a chain of chemical reactions of binding on one side and releasing on the opposite side of the membrane (Lemieux et al. 1990). Translocations of mobile *X*-channels over the cell surface was possible by way of lateral diffusion and electrophoretic drift (Hille 1992; Singer 1975; Fromherz and Zimmermann 1995).

This model was described by the system of four uni-dimensional reaction-diffusion equations of four macroscopic variables: the transmembrane potential; the submembrane concentration of *X* cations; the density of *X*-channels in both open and closed states; and the density of open *X*-channels. One dimension was sufficient since in a long narrow cylindrical domain ($d \ll l$), any solution of the reaction-diffusion system was shown to asymptotically lose its transectional/circumferential dependence (Kurata et al. 1989).

The first equation of the model was the non-linear cable equation giving the relationship between local transmembrane potential and currents:

$$\frac{\partial \psi}{\partial t} = \frac{d}{4 R_{in} C_m} \frac{\partial^2 \psi}{\partial z^2} + Q_\psi(\psi, \rho, [X]_i), \qquad (1)$$

where the non linear source function Q_ψ included four components of the transmembrane current:

$$Q_\psi(\psi, \rho, [X]_i) = -(J_X(\psi, \rho, [X]_i) + J_Y(\psi) + J_L(\psi) + J_p(\psi, [X]_i))/C_m .$$

The passive *X*-current (see Eq. (A.1.1) in Appendix 1 for details) depended on the density of open *X*-channels ρ, which was changed owing to voltage-dependent conformational transitions. The kinetics of these transitions were

described by the following equations:

$$\frac{\partial \rho}{\partial t} = Q_\rho(\psi, \rho, e),$$
$$Q_\rho(\psi, \rho, e) = \alpha(\psi)(e-\rho) - \beta(\psi)\rho, \quad (2)$$

where $\alpha = L_+ \exp[\psi(1-\gamma)]$ and $\beta = L_- \exp(-\psi\gamma)$ are voltage-dependent rate constants; L_+ and L_- are the values of the rate constants for $\psi = 0$; and $\gamma \in [0, 1]$ is the dimensionless parameter characterizing voltage dependence of the forward and backward conformational transitions. Only the activation kinetics for open-closed transitions were considered because we focused on the phenomena occurring under small deviations (±5 mV that is $\Delta\psi = \pm 0.2$) from the resting membrane potential ($\psi = \psi_{st}$). The transition kinetics of sodium channels of inward current in this range of voltages (−40 to −60 mV) were dominated by activation rather than by inactivation. In (2) we used the partial time derivative of ρ because it also changed along z as a result of lateral diffusion and drift of the channels in the membrane. The electrodiffusion of the whole population of mobile open and closed X-channels was described by the Nernst-Plank equation (Fromherz and Zimmermann 1995):

$$\frac{\partial e}{\partial t} = D_e \frac{\partial^2 e}{\partial z^2} + Q_e(\psi, e),$$
$$\text{with} \quad Q_e(\psi, e) = D_e N_e \frac{\partial}{\partial z}\left(e \frac{\partial \psi}{\partial z}\right). \quad (3)$$

The fourth dynamic variable $[X]_i$ changed owing to transmembrane transfer of X-cations, their axial diffusion in the submembrane layer and exchange with the deeper cytoplasm. This was described by the following equation:

$$\frac{\partial [X]_i}{\partial t} = D_X \frac{\partial^2 [X]_i}{\partial z^2} + Q_X(\psi, \rho, [X]_i) \quad (4)$$

with the source function

$$Q_X(\psi, \rho, [X]_i) = -\frac{\beta}{\chi F}(3J_p + J_X) + P_X([\tilde{X}]_i - [X]_i). \quad (5)$$

The first term in (5) explicitly incorporates the contributors to the transfer of X across the membrane. They are the pump current density $3J_p$, defined by (A.1.2), extruding 3 cations per cycle (as Na^+-K^+ ATPase does, for example) and the passive X-current density J_X. However, the factor of J_p can be other than 3 for other active transport mechanism. The second term described ion exchange between the submembrane layer and the bulk intracellular space.

3 Analysis of diffusion driven instability

In this section we show that the model generated the steady-state non-uniform spatial distribution of the resting membrane potential, density of channels and ion concentrations.

To analyze the model, we followed the approach of Turing (1952). First, we determined conditions of stability of the system in relation to the spatially homogeneous perturbation, which were also the conditions of stability of the point system (Murray 1989). Then we determined the conditions of instability in relation to spatially inhomogeneous perturbations (the diffusional or Turing instability). This allowed us to specify the model parameters for obtaining the illustrative numerical results.

We have shown that the necessary and sufficient condition for the existence of *DSs* is the following inequality (see the Appendex 2 for details):

$$\Phi(k^2) = -D_e k^2 (A k^4 + B k^2 + C) < 0, \quad (6)$$

where

$$A = D_\psi D_X m_{22},\ B = -(D_\psi A_{11} + D_X A_{33} + D_X e_{st} N_e m_{12} m_{24}),$$

and

$$C = e_{st} N_e m_{24}(m_{12} m_{33} - m_{13} m_{32}) + Det(M),\ D_\psi = d/(4 R_{in} C_m),$$

where k is the wave-number defining period of the spatial pattern ($k = \pi n/l$, n is integer), m_{ij} are the linearization coefficients, and A_{11}, A_{22}, and A_{33} are the minors of the elements m_{11}, m_{22}, and m_{33}, respectively (see Appendix 2).

Consider the conditions when (6) holds. Because $D_\psi > 0$, $D_X > 0$ and $m_{22} = \partial Q_\rho/\partial\rho = -(\alpha + \beta) < 0$ always hold, A is always negative. Because $D_\psi A_{11} \gg D_X A_{33}$ and $Det(M) < 0$ the DSs do not occur if the following two conditions are both false:

$$D_\psi m_{22} m_{33} + D_X e_{st} N_e m_{12} m_{24} < 0, \quad (7a)$$
$$e_{st} N_e m_{24}(m_{12} m_{33} - m_{13} m_{32}) > 0, \quad (7b)$$

since in this case (6) also does not hold.

Consider now the necessary conditions for (6). Since $m_{22} < 0$, $m_{12} = \partial Q_\psi/\partial\rho = -J_X/C_m\rho_{st} > 0$ and $m_{24} = \alpha > 0$ always hold, (7a) can only be true when at least one of the conditions $m_{33} > 0$ (the positive feed-back exists) or $N_e < 0$ hold. The inequality $m_{33} > 0$ is true in the case when $\partial Q_3/\partial[X]_i > 0$, which is possible when $P_X < 0$ and/or $3\partial J_p/\partial[X]_i < \partial J_X/\partial[X]_i$. Physiologically, $\partial J_p/\partial[X]_i > 0$ and $\partial J_X/\partial[X]_i < 0$. The condition $P_X < 0$ means that there is an increase of submembrane concentration $[X]_i$ due to flux of X-cations from the deeper layers but not across the membrane. Putting the values of the linearization coefficients into (7b) gave the inequality:

$$\partial J_X/\partial\rho\,[2\partial J_p/\partial[X]_i - P_X] < 0.$$

Thus, the necessary condition (7b) holds only when the inequalities $\partial J_p/\partial[X]_i > 0$ or $P_X < 0$ are true because of $\partial J_X/\partial\rho < 0$.

Hence, on the basis of linear analysis of stability we concluded that the existence of *DSs* was possible only when at least one of the following conditions held:

(i) $3\partial J_p/\partial[X]_i < -\partial J_X/\partial[X]_i$ with $\partial J_p/\partial[X]_i > 0$ and $\partial J_X/\partial[X]_i < 0$ meaning that an increase in $[X]_i$ should activate the pumps and inhibit the channels, and the rate of the pump activation should be lower than that of the channel inhibition;
(ii) $N_e < 0$, meaning that the molecule forming X-channels should bear negative electrophoretic charge exposed to the intracellular space;

(iii) $P_X<0$, meaning that *X*-cations induce the release of further *X*-cations from intracellular stores (this was not the case for the specific model under study, but it may hold in other systems – see Discussion).

Thus, to answer the question about the possibility of the creation of DSs, one should first check the above conditions (i – iii). If none of them hold, then DS does not occur. If at least one of them holds, then (7) should be checked. If at least one of the conditions (7) holds, then (6) should be checked to get the final answer.

The bifurcation value of the wave number was defined as $k_b^2=-B/2A$, with the parameters, *A* and *B* obeying the equation $B^2-4AC=0$ obtained from (6). This resulted in:

$$k_b^2=\frac{m_{33}}{2D_S}+\frac{m_{11}}{2D_\psi}+\frac{m_{12}}{2D_\psi m_{22}}(e_{st}N_e m_{24}-m_{21}).$$

Putting the linearization coefficients in this equality gave the number of periods of the pattern

$$n=\frac{l k_b}{\pi}=\frac{l}{\pi\sqrt{2C_m}}\sqrt{\frac{-G_m+I_X\left(N_e-\frac{\alpha}{\alpha+\beta}\right)}{D_\psi}+\frac{m_{33}}{C_m D_X}}, \quad (8)$$

where G_m is the total membrane conductivity including *X*- and *Y*-conductivities, the leak conductivity G_L and the conductivity of the pump Λ. As followed from this formula, the number of periods of *DSs* occurring in the cell with mobile channels differed from that in the same cell with immobile channels, $n=\frac{l}{\pi\sqrt{2C_m}}\sqrt{-\frac{G_m}{D_\psi}+\frac{m_{33}}{C_m D_X}}$. This new periodicity depended on the electrophoretic charge N_e and the current I_X of these channels. Depending on negative or positive values of N_e the electrophoretic mobility of the channels worked as a positive or negative feedback mechanism, respectively. The formation time of the spatial pattern was much shorter than necessary for the channel installation into or release from the plasma membrane. In this case, the average density of *X*-channels, e_{st}, remained unchanged during the time of the pattern formation.

The linear analysis allowed us to obtain the sufficient conditions (6) for creation of *DSs* in cylinder-shaped cells. Because of the big differences between the diffusion coefficients this analysis did not allow us to predict the spatial forms of *DSs*. In this case the general solution usually included many harmonics with different wave numbers. One can estimate amplitudes and stability of the *DSs* only by non-linear analysis.

Results

Computer simulations were performed to study the shape of steady *DSs* far from equilibrium and to check the conditions for the creation of *DSs*, which were determined using analytical methods. Numerical solutions of (1–4) with sealed-end boundary conditions were obtained using the Crank-Nicholson method (Peaceman and Rachford 1955).

For specific numerical examples, we considered Na^+ and K^+ as *X*-type and *Y*-type cations, respectively. However, the suggested mechanism can involve other ion species, provided that the above derived conditions of diffusion driven instability are obeyed.

Λ was equal to 1 when the surface density of the pump sites is about 500 μm^{-2} (Lemieux et al. 1990). When the values of $[\bar{X}]_i=5.4$ mM and $\bar{\Lambda}=1$ $\mu S/cm^2$ were fixed then the current densities (A.1.4) measured in units of $\mu A/cm^2$ (F/RT) were $J_p^0=0.121$, $J_p^{-\infty}=-0.01$, and $J_p^{+\infty}=0.13$ (Lemieux et al. 1990) and the function describing concentration dependence of the pump current was $f([X]_i)=(0.6\times10^{-3})/(1-3/[X]_i+5/[X]_i^2)$.

The initial conditions consisted of small, uniformly distributed random perturbations of ψ, $[X]_i$, e, ρ from their steady-state values.

1 Bifurcation analysis

With the parameters listed in the Table 1 the pattern was mainly determined by the conductivity of the pump Λ, and by the electrophoretic charge of *X*-channels N_e. To study the influence of local kinetics on pattern formation we computed a family of plots of the $\Phi(k^2)$ function as defined by (6) for fixed $N_e=0$ and different values of Λ as the parameter (Fig. 1A). From these plots the bifurcation value $\Lambda_b=2.54$ $\mu S/cm^2$ corresponded to $\Phi(k^2)=0$. In these conditions the pattern occurred with a single unstable mode having the bifurcation wave number $k=k_b=0.033$ μm^{-1}. The pattern had the form of strata, the number of which was $n=l k_b/\pi=4$ for $l=375$ μm. For the super-critical $\Lambda=2.6>\Lambda_b$ a set of unstable modes with the wave numbers *k* in the range of 0.035 to 0.044 μm^{-1} occurred. For sub-critical $\Lambda=2.5<\Lambda_b$ there were no unstable modes and

Table 1 Parameters of the model

Symbol	Value	Source
l	375 μm	
d	0.4 μm	
χ	0.05 μm	
e_{st}	300 μm^{-1}	(Hille 1992)
σ_{Na}	14 pS	(Sherman et al. 1990)
G_K	0.02 mS/cm^2	
P	0.56 mM^{-1}	(Sherman et al. 1990)
G_L	0.002 mS/cm^2	(Jack et al. 1983)
ψ_L	−2.1	(Jack et al. 1983)
C_m	1 $\mu F/cm^2$	(Jack et al. 1983)
R_{in}	40 Ω · cm	(Jack et al. 1983)
$[Na^+]_o$	150 mM	
$[K^+]_o$	14 mM	
$[K^+]_i$	114 mM	
γ	0.1	(Hille 1992)
L_+	1.394 ms^{-1}	
L_-	0.791 ms^{-1}	
P_{Na}	0.5 s^{-1}	

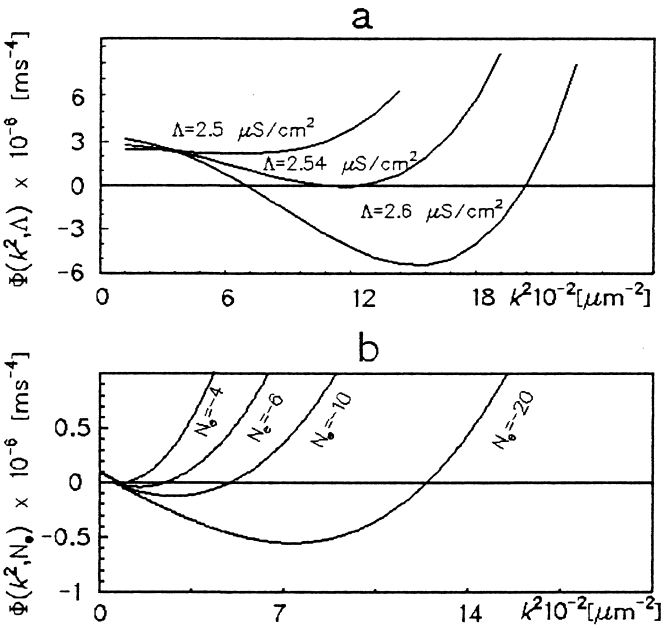

Fig. 1 Bifurcation diagrams of the free term of the characteristic equation (6) $\Phi(k^2)$ as a function of the wave number k and of the two parameters Λ and N_e plotted for different values of Λ at fixed $N_e = 0$ (**a**) and for different N_e at fixed $\Lambda = 2.5$ (**b**)

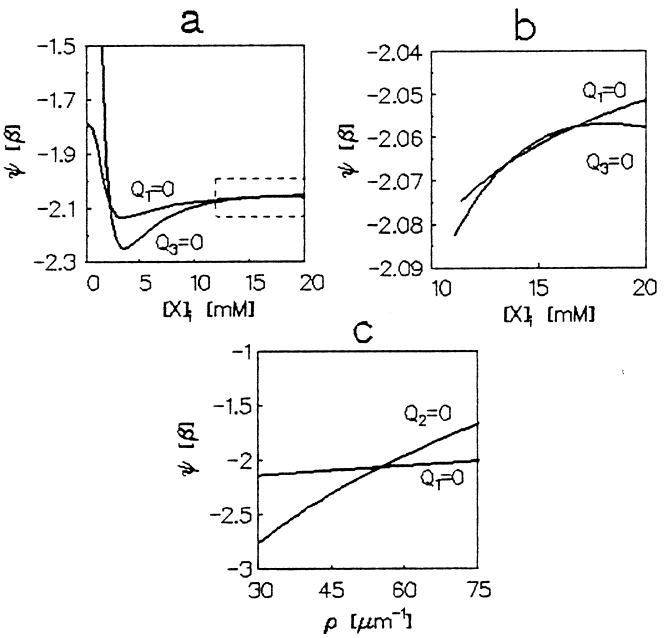

Fig. 2 Null-isoclines of the phase portrait of the model in the planes $\rho = \rho_{st}$ (**a**, **b**) and $[X]_i = [X]_{st}$ (**c**). $Q_1 = 0$, $Q_2 = 0$ and $Q_3 = 0$ are null-isoclines of the rates of change in the transmembrane potential ψ, the density of open channels ρ, and the ion concentration $[X]_i$, respectively, with steady state coordinates (ψ_{st}, ρ_{st}, $[X]_{st}$). Part of (**a**) within the dotted box is given in (**b**) on a larger scale

the pattern was absent. Thus, by changing Λ some different forms of the pattern formation were obtained.

Computations of $\Phi(k^2)$ with $\Lambda = 2.5 < \Lambda_b$ and non-zero N_e as parameters allowed us to estimate the contribution of electrophoretic mobility of the channels to the pattern formation (Fig. 1B). *DSs* emerged in the system with sub-critical Λ when N_e exceeded the critical value of about −4.

2 Phase portrait

Conditions for pattern formation in the system were illustrated by the phase portrait of the latter in the vicinity of the steady state. Consider a simpler case of $N_e = 0$ (electrophoretically neutral channels) and $\Lambda = 2.6$ exceeding the bifurcation value Λ_b. In this case the conditions of stability of the point system (A.2.5) held. The conditions of diffusive instability also held when the inequality $D_\psi \gg D_X \gg D_e$ held ($D_\psi = 25\,000$, $D_X = 0.1$, and $D_e = 0.0001\ \mu m^2/ms$). With $N_e = 0$ a set of only three equations ((1), (2), and (4)) remained for the analysis of the local model. In this case the phase portrait of the point system determined the kinetics of formation of *DSs* (Nicolis and Prigogine 1977). Figure 2 shows null-isoclines plotted in the planes ψ vs. $[X]_i$ (a), (b) and ψ vs. ρ (c). The point with the coordinates $\psi_{st} = -2.057$ (−51.43 mV), $\rho_{st} = 55\ \mu m^{-1}$, and $[X]_{st} = 16.63$ mM corresponded to the local steady-state of the system. This state was stable in relation to fluctuations of ψ and ρ, as one can see from the null-isoclines shown in Fig. 2c. This meant that the system tended from an arbitrary initial state (ψ, ρ) to its stationary point. When $\psi = \text{const}$ and $\rho = \text{const}$ the fluctuations of $\delta[X]_i$ increased (Fig. 2b), i.e. in the phase plane ($[X]_i$, ψ) the limit-cycle oscillations might occur in the neighborhood of the local steady state. This is very important, since the system in this case was unstable in relation to spatially non-uniform perturbations. Thus, the system reacted in a different way to fluctuations in different state variables. Under some conditions, the *DSs* were created owing to accumulation of *X*-cations in the submembrane layer without lateral electrodiffusion of the ion channels.

3 Super-critical pump conductance, electrophoretically neutral channels

Numerical computations of the model equations have shown that when spatially inhomogeneous perturbations of ψ, ρ, and $[X]_i$ were introduced as initial conditions then the *DSs* were formed with the longitudinal profiles shown in Fig. 3 and Fig. 4.

The initial condition played a role in determining whether a specific pattern will emerge. We used small random perturbations about the uniform steady state (white noise) as the initial condition. In this case, all modes were present, but only those corresponding to the unstable wavelengths band, were augmented. The mode with the minimum $\Phi(k^2)$ and maximum wave-length (see Fig. 1 for example) was the fastest growing and ultimately it dominated in the steady state persisting inhomogeneous pattern.

Figure 3 shows how the initial white noise perturbation with all spectral modes (Fig. 3 a) transformed in the course of the pattern formation. The non-linear system selected the long-wave modes and by 200 ms the modes $n=4$ and $n=5$ dominated (Fig. 3 b). Later the spectrum shifted to the longest-wave range with dominating modes $n=1$ and $n=4$ (Fig. 3 c). In the final pattern a single dominating mode with $n=4$ survived (Fig. 4). The spatial patterns for ψ and ρ were nearly sinusoidal, whereas that for $[X]_i$ was in the form of strata with rather sharp edges. The number of the strata $n=4$ corresponded to that predicted by the bifurcation analysis.

4 Sub-critical pump conductance, electrophoretically charged channels

When $\Lambda=2.5\ \mu S/cm^2$ was sub-critical the pattern could still be formed if the channels bore some electrophoretic charge. For the model parameters as above, the critical value of $N_e=-4$ was found. The pattern generated for super-critical electrophoretic charge $N_e=-20$ is shown in Fig. 5. The pattern was different from that in Fig. 4 in several respects. The coupled distributions of the field variables had three maxima in the same spatial domain. Spatially periodic longitudinal distributions of e and ρ were stratified with more sharp peaks of distributions of e.

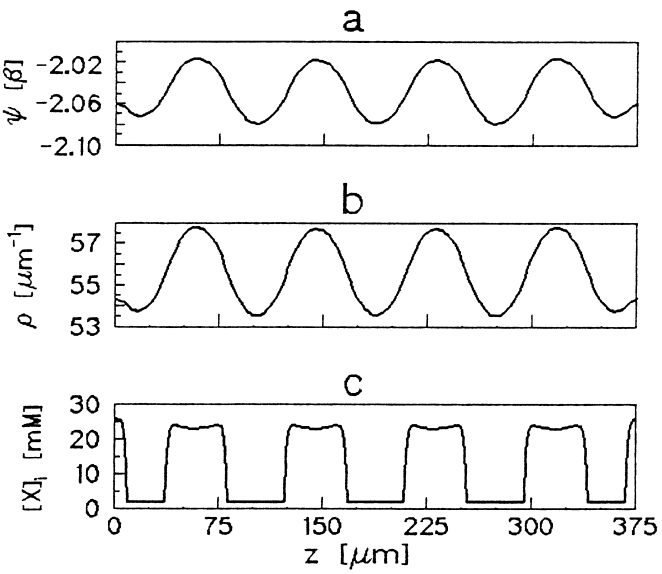

Fig. 4 Inhomogeneous steady-state distributions of the transmembrane potential (**a**), the density of open X-channels (**b**) and the intracellular concentration of X-cations (**c**) along the cylinder-shaped cell. The parameters were the same as for Fig. 3

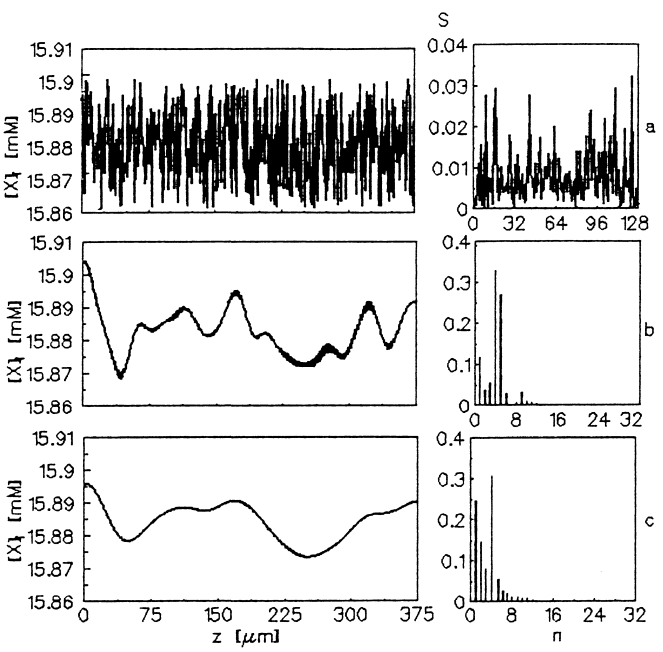

Fig. 3 a–c Spatial distributions of the intracellular concentration of X-cations along the cylinder-shaped cell (*left*) and the corresponding spatial Fourier spectra (*right*) at different time: **a** $t=0$ ms, **b** $t=200$ ms and **c** $t=500$ ms. S is the normalized spatial power spectrum, and n is the number of the mode. The channels had no electrophoretic charge ($N_e=0$). The bifurcation parameter $\Lambda=2.6\ \mu S/cm^2$ was super-critical. Other parameters are given in the text and Table 1

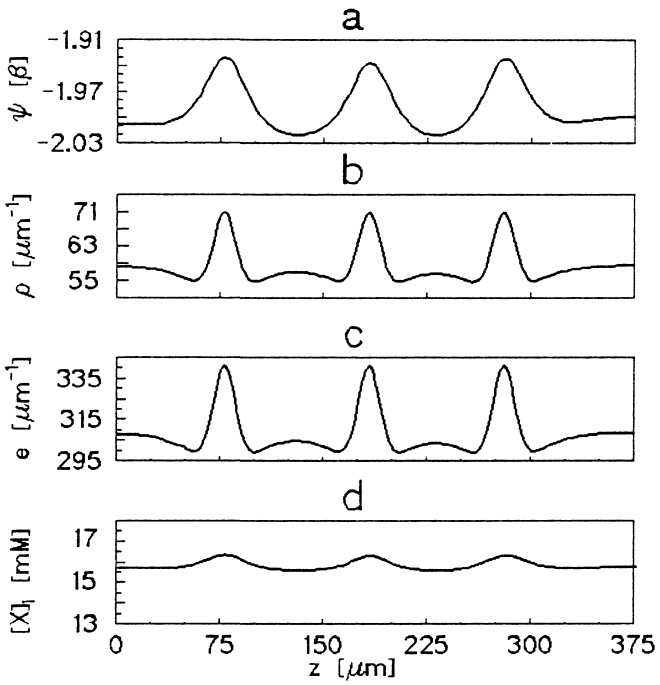

Fig. 5 Inhomogeneous steady-state distributions of the transmembrane potential (**a**), the densities of X-channels in only open (**b**) and in both open and closed states (**c**), and the intracellular concentration of X-cations (**d**) along the cylinder-shaped cell. The channels bore electrophoretic charge $N_e=-20$ exposed to the intracellular space. Bifurcation parameter $\Lambda=2.5\ \mu S/cm^2$ was sub-critical. Other parameters are given in the text and Table 1

Corresponding peaks of ψ merged more smoothly into each other, and those of $[X]_i$ were hardly seen. The results of this experiment allowed us to notice that in the system with cross-diffusion the *DSs* may occur without auto- or cross-catalysis. In this respect, the model under investigation differed from those described by the system of parabolic equations without cross-diffusion where *DSs* were created owing to either autocatalysis $m_{ii}>0$ (Nicolis and Prigogine 1977) or cross-catalysis $m_{ij}>0$, $i\neq j$ or to both (Kerner and Osipov 1990; Savtchenko and Korogod 1994).

5 Super-critical pump conductance and electrophoretic charge of channels

When both $\Lambda=2.6$ μS/cm^2 and $N_e=-20$ were super-critical the *DSs* were created owing to both accumulation of *X*-cations in the submembrane layer and lateral electrodiffusion of *X*-channels. The pattern is shown in Fig. 6. Under these conditions there were 11 peaks in the distributions, which were nearly sinusoidal for ψ, ρ, and e, whereas $[X]_i$ was distributed in strata with sharp edges (cf. Fig. 4).

6 Sub-critical pump conductance and electrophoretic charge of channels

With $\Lambda=2.5$ μS/cm^2 and $N_e=0$ neither of the necessary conditions of the necessary and sufficient conditions for the pattern formation were obeyed. In this case, the initial spatially non-uniform perturbations relaxed in time, and the system tended to its spatially uniform state (not illustrated).

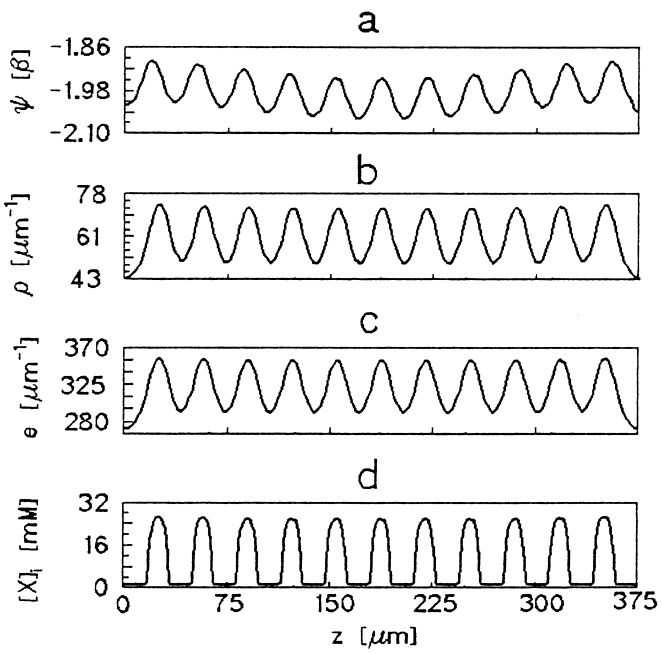

Fig. 6a–d Same as Fig. 4 but with super-critical $\Lambda=2.6$ μS/cm^2

Discussion

1 Justification of the model and the parameters

Statement of the problem of simulation studies of self-organization phenomena in the neuron is justified by some prerequisites for the formation of *DSs* in these cells. These prerequisites are similar to those found in other non-linear systems: the neuronal membrane is an open physical and chemical system involved in substance and energy exchange with the environment (Hille 1992); there is a dissipation of chemical energy of active transmembrane transport, and it is used for maintenance of non-equilibrium steady distribution of the ions between intra- and extracellular media; there is a possibility of spatial redistribution of the main components of the system, namely the ions and the channels, due to electrodiffusion of the ions in the submembrane layers (Qian and Sejnowski 1989) and lateral diffusion of the channels in the fluid mosaic membrane (Singer 1975), respectively.

Our model includes three longitudinal "field" variables, the transmembrane voltage, the density of electrophoretically charged channels of inward current and the submembrane concentration of cations carrying this current. These three variables are electrically coupled but they are rather different in their rates of spatial relaxation. In this model, we observed some spatial patterns of the channels similar to those obtained by Fromherz (Fromherz and Zimmermann 1995) in two field variables, the channel density and the potential. Fromherz's model did not include kinetics of open-closed voltage-gated transitions of ion channels and changes in the ion concentration. The assumption that all ion channels have only one conformational state critically influences the condition of creation of DSs, as the bifurcation value of electrophoretic charge must be much greater than that in our model with conformational transitions.

According to our estimations, the spatial pattern could be developed on the time scale of 10–100 min. Spatial perturbations of voltage relax most rapidly, and therefore cannot be the major reason for patterning even if the voltage is a local activation variable. Perturbations of the local ion concentration and the density of the channels are more suitable candidates. The emphasis should be put on the currents which produce sufficient changes in the ion concentrations. Naturally, they are inward currents bringing ions into the restricted volume of intracellular space, rather than outward currents to the bulk of extracellular media of unmyelinated neuronal processes. The effect is more pronounced when in the restricted intracellular volume the concentration of ions conducting inward current is much lower than the extracellular concentration. This is the case in the neuron, where the inward current is conducted by Na^+, and the outward one by K^+. Consequently, the activation kinetics of the latter are not described in detail, and changes in $[K]_o$ are not taken into account. For the channels considered here, the densities are important model parameters. They are chosen from the estimates given on pp 329–331 of Hille (1992).

2 Mechanisms of pattern formation in different conditions

The necessary conditions of the necessary and sufficient conditions (6) for the pattern formation were obtained from the linear analysis and confirmed further by the results of corresponding numerical computations performed with the complete non-linear model. On the basis of the results shown in Figs. 1 – 6 we suggest the following mechanisms for pattern formation in the cylinder-shaped neuronal process under different conditions.

A Intracellular ion electrodiffusion as leading process

When the channels are electrophoretically neural ($N_e=0$) then their lateral electrodiffusion does not participate in formation of the pattern shown in Fig. 4, and the density of channels *e* remains uniformly distributed over the neurite (not shown). Consider a depolarizing fluctuation of the local voltage. This activates *X*-channels and increases the influx of *X*-cations and $[X]_i$. Such an increase may switch on a positive feed-back mechanism which is critical for creation of *DSs*. If extrusion of *X*-cations by the pump under these conditions is not sufficient to overcome passive inflow through the increasing number of open *X*-channels then $[X]_i$ increases further. All other positive feed-back mechanisms corresponding to positive terms in (7) are not critical for creation of *DSs*.

When the local concentration of *X*-cations is increased, then the negative feed-back mechanisms corresponding to negative terms in (7) are switched on. Electrodiffusion of the ions is the only critical negative feed-back for creation of *DSs*. Thus, the coupled non-uniform distribution of the density of open channels and of the submembrane ion concentration can create conditions sufficient for maintenance of an inhomogeneous distribution of the membrane potential at the expense of potential- and concentration-dependent energy dissipation in active ion transport systems.

We considered sodium as the ion conducting inward *X*-current, that determined the positive value of P_X. However, P_X can be negative in other cases, e. g. when the *X*-ion is calcium. Negativity of P_X corresponds to Ca^{+2}-induced release of Ca^{+2} from the intracellular stores (Tsien and Tsien 1990) leading to a further increase in the local hyperpolarization of the plasma membrane.

B Lateral electrodiffusion of channels as leading process

Consider local depolarization occurring as a result of fluctuation. This also turns on several feed-back mechanisms. If *X*-channels have negative electrophoretic charge ($N_e<0$), then they drift to the depolarization zone and thus contribute to an increase in the local density of the channels in both conformational states. The inward current through the increasing number of open channels further depolarizes the membrane. This local positive feed-back is critical for creation of *DSs*. Another important but not critical positive feed-back is due to opening (activation) of the closed channels by increasing local depolarization. In these conditions, intracellular current flowing away from the depolarization zone tends to relax the longitudinal potential gradient and serves as a critically important spatial negative feed-back. Another important but not critical negative feed-back is thermal lateral diffusion of the channels. There is a competition between the mentioned positive and negative feed back mechanisms influencing the spatial pattern of the transmembrane potential. Creation of DSs is determined by the interplay between the critical competitors.

C Cumulative effects

If only one critical positive feed-back mechanism participates in formation of *DSs*, then the scenario of the self-organization process is determined exclusively by the intrinsic parameters of the system. If two positive feed-back mechanisms are critical, then the sequence of switching on these mechanisms is important for creation of *DSs* in addition to the intrinsic parameters. In this study, both critical positive feed-back mechanisms of self-organization were switched on simultaneously and the features of the pattern formation were determined by a significant difference in the diffusion coefficients of the channels and the ions. The diffusivity of the ions in the submembrane layer is about 1000 times greater than that of the channels in the membrane matrix; hence during the first 100 s the formation of the *DSs* was performed practically by the scenario described in section *B*. The *DS* formed in 100 s was similar to that shown in Fig. 4. However, this structure was not finally stabilized and continued to slowly deform as the result of electrodiffusion of the channels. The channels carrying the intracellularly exposed negative electrophoretic charge moved to the depolarization zones, thus increasing the local inward current and the depolarization. As a result of this the new DS occurred during more than 60 min with a greater amplitude and a shorter spatial period than in the two previous cases (sections *A* and *B*).

3 Model assumptions and their influence on pattern formation

Although it is disputable which proportion of each population of the membrane proteins is mobile (Hille 1992; Peters 1981), one population here (the channels of inward current) is totally mobile, whereas others (the channels of outward current and the pump molecules) are immobile. For the pattern formation this assumption is not critical, but it does put restrictions on possible spatial dynamics and pattern of ion channels. For the pattern formation the most important is the sign of the product $N_e I_X$ [see Eq. (8)] defining the feed-back mechanism. If $N_e I_X>0$ then the electrophoretic mobility plays the role of the positive feed-back and vice versa. Consider, for example, the case when both kinds of the channels, $X=Na^+$ and $Y=K^+$, are mobile.

An inward current through *Na*-channels and an outward current through *K*-channels induce positive and negative local perturbation of the membrane potential, respectively. If both kinds of channels bear the same electrophoretic charge, $N_e < 0$ and have the same diffusion coefficient, D_e, then *Na*-channels are attracted and *K*-channel are repulsed by other *Na*- and *K*-channels, because $N_e I_{Na} > 0$ and $N_e I_K < 0$ due to the electrical field. In this case the final coherent pattern is defined by a competition between spatial dynamics of these kinds of channels.

Another assumption of the model is the initial condition, which is known to play a role in determining whether a specific pattern will emerge (Murray 1989). If the initial condition is random perturbation about the uniform steady state (white noise) in which all modes are present, then the final pattern is defined by intrinsic properties of the nonlinear system. The modes are amplified or suppressed depending on whether or not they are in the unstable band of wavelengths as determined by the system parameters. We have chosen this type of initial condition since we are interested in the intrinsic potency of the neuronal dendrites for the pattern formation. However, the pattern formation is also possible when the perturbation from the uniform steady state is initiated at one end of the dendritic cylinder, as in the case of the action potential generated at the soma. In this case, the spatial pattern develops from there, eventually spreading throughout the whole domain. If the domain of the initial perturbation is so small that its wavelengths are short and do not belong to the unstable band, then the final pattern contains the smallest wavelength. Thus, the specific pattern that evolves for a given mechanism depends on how the instability is initiated.

4 Neurobiological consequences

Computer simulation studies provide a useful complementary tool for studies of non-uniform spatial distributions of ions, channels, and voltages over the neurons. Direct studies of these distributions in natural experiments meet both methodological and technical difficulties (for reviews see e.g. Johnston et al. 1996; Yuste and Tank 1996). Investigation of spatial voltage patterns with microelectrodes and voltage-sensitive dyes is complicated by the facts that microelectrode recordings provide space integral (superposition) of voltage from many sources of unknown distribution, and the recently available optical recordings provide a mosaic of time integrals over patches of the cellular membrane unevenly oriented in relation to the recording device. Lateral distribution of channels can only be studied when they are labeled with marker-molecules, therefore one needs evidence that the marker does not change the behavior of the channels. Optical imaging of intracellular ion concentration profiles is complicated by the problem of mutual distribution and interaction of the ions and the ion-sensitive dye. Despite the difficulty of direct correspondence between the natural and computer experiments, several important physiological aspects of our simulation results must be stressed.

First, the maintained non-uniform distribution of the membrane potential and the local ion concentrations can be a factor which controls the state (and probably weight) of synapses located on the membrane through spatial modulation of the electrochemical potential of the ions. The postsynaptic effect of the same presynaptic intensity may be different depending on the location of the synapse at the site of the maximum or minimum of the distributions. This spatial modulation is dynamic and may therefore be a basis of postsynaptic plasticity in morphologically static presynaptic arrangement.

Second, the inhomogeneous lateral distributions of the ion channels, especially with the sharp-edge strata allows one to consider them as an example of spatially periodic "hot spots" (Bacskai et al. 1995; Shaw et al. 1994). An important conclusion is that these ultrastructural phenomena may occur as a result of self-organization phenomena within the population of mobile channels, rather than as genetically pre-programmed positioning. Long lasting self-maintenance of this arrangement of the membrane proteins may be sufficient for chemical reactions of their anchoring to the cytoskeleton. Recent studies gave evidence of inhomogeneous distribution of the specific membrane resistance, R_m, over the neuron with lower values for the soma and greater values for the dendrites (Pongracz et al. 1991). Moreover, R_m (and hence its reciprocal, the specific membrane conductance, G_m) may vary smoothly along the dendrites or may be subject to sharp local changes, forming so-called "hot spots" (Bacskai et al. 1995), which are the sites of local increase of the membrane conductance. Since the total membrane conductance is the sum of conductances of single ion channels, it is worthwhile to analyze mechanisms of inhomogeneous distribution of $R_m = 1/G_m$ in terms of distribution and redistribution of the channels (Llinas 1988). This analysis may also elucidate mechanisms of inhomogeneous distribution of intracellular cations and lead to revision of a common view on homogeneity of the resting transmembrane potential.

Third, inhomogeneous distribution of dendritic conductances provided by the channels is thought to have consequences for the temporal pattern of dendritic integration and output response, although the specific role of active conductances found throughout the dendritic trees (e.g. in pyramidal cells of the hippocampus and neocortex and Purkinje cells of the cerebellum) "remains a mystery", as concluded in the review by Yuste and Tank (1996). As follows from concentration imaging with the Na^+ and Ca^{2+} sensitive dyes and from patch-clamping experiments, there is inhomogeneous distribution of influx of these ions between the soma and the dendrites, and over the dendrites (Lav-Ram et al. 1992; Jaffe et al. 1992; Stuart et al. 1993; Sprus-ton et al. 1995; Magee and Johnston 1995). One cannot conclude whether or not the dendritic distribution of the conductances is patterned. However, the authors often discuss the consequences of the channel density for forward and backward propagation of action potentials in the dendrites. One can assume, that as a consequence of band-like condensation of mobile sodium channels due to mechanisms suggested in this paper, the active properties of the

dendrites can change from weakly regenerative to more strongly regenerative (Johnston et al. 1996). Extension of these insights to the calcium channel population can offer a possible explanation for clustering of Ca^{2+} channels within the area of membrane containing active calcium conductances which could give rise to punktate Ca^{2+} (Lankaster and Zuker 1994).

Last, maintained non-uniform distribution of the surface density of ion channels (and probably other receptor membrane proteins) can underlie morphogenetic events (e. g. shaping, process outgrowth etc.). The crucial point is that these distributions, being *DSs*, depend on the intrinsic system parameters (process diameter, mean channel density, the length and time constants etc.), but not on external influences.

Acknowledgements We are grateful to Dr. S. Tyč-Dumont for support, encouragement and valuable discussions. This work was supported by Dniepropetrovsk State University, Ukraine (grant No 79–95) and by Centre National de la Recherche Scientifique, France (PICS No 231).

Appendix 1

The model used in the work has the following form.

Expressions for passive currents of X and Y cations were

$$J_X(\psi, \rho, X_i) = \frac{\sigma_X \rho P \psi}{\pi d} \frac{[X]_o - [X]_i \exp(\psi)}{1 - \exp(\psi)} \qquad \text{(A.1.1)}$$

and

$$J_Y(\psi) = G_Y P \psi \frac{[Y]_o - [Y]_i \exp(\psi)}{1 - \exp(\psi)}, \qquad \text{(A.1.2)}$$

respectively. Equations (A.1.1) and (A.1.2) were written on the basis of the theory of constant field (Goldman 1943).

The leak current was a function of the transmembrane potential:

$$J_L(\psi) = G_L(\psi - \psi_L). \qquad \text{(A.1.3)}$$

The pump current or active transport of X cations against their electrochemical gradient was described as follows:

$$J_p(\psi, [X]_i) = \Lambda \frac{a_1 \exp(\psi) - a_2 \exp(-\psi)}{a_3 \exp(\psi) + \exp(-\psi)} f([X]_i), \qquad \text{(A.1.4)}$$

where $f([X]_i)$ is the function describing the dependence of the pump current on $[X]_i$. This function is characterized by a curve with maxima, such that the pump extrusion is absent when $[X]_i$ is zero (Garrahan and Garay 1974). This behavior was described as follows: $f([X]_i) = a/(b + c/[X]_i + d/[X]_i^2)$ which is similar to the equation for the of kinetics of enzyme-substrate reactions. Equation (A.1.4) was that derived in Lemieux et al. (1990) using the method of King and Altman. The limiting equations,

$$J_p(0, [\bar{X}]_i) = J_p^0, \quad J_p(-\infty, [\bar{X}]_i) = J_p^{-\infty},$$
$$\text{and} \quad J_p(+\infty, [\bar{X}]_i) = J_p^{+\infty}$$

allowed us to define the parameters of (A.1.4) as follows:

$$a_1 = \frac{J_p^{+\infty}(J_p^{-\infty} - J_p^0)}{\bar{\Lambda} f([\bar{X}]_i)(J_p^0 - J_p^{+\infty})}, \quad a_2 = \frac{J_p^{-\infty}}{\bar{\Lambda} f([\bar{X}]_i)},$$

$$\text{and} \quad a_3 = \frac{J_p^{-\infty} - J_p^0}{J_p^0 - J_p^{+\infty}},$$

where $\bar{\Lambda}$ and $[\bar{X}]_i$ are constants. The pump current, $J_p(\psi, [X]_i)$ was considered as electrogenic with extrusion of three X ions and uptake of two Y ions in each cycle.

Appendix 2

The basic equations (1–5) were re-written in the unified form:

$$\frac{\partial x_j}{\partial t} = D_j \frac{\partial^2 x_j}{\partial z^2} + Q_j, \quad j = 1, 2, 3, 4, \qquad \text{(A.2.1)}$$

where $x_1 = \psi$, $x_2 = \rho$, $x_3 = [X]_i$, $x_4 = e$; $Q_1 = Q_\psi$, $Q_2 = Q_\rho$, $Q_3 = Q_X$, $Q_4 = Q_e$; $D_1 = D_\psi = d/(4R_{in}C_m)$, $D_2 = 0$, $D_3 = D_X$, $D_4 = D_e$. For Eqs. (A.2.1) the "sealed-end" boundary conditions were used:

$$\frac{\partial x_j}{\partial z} = 0, \quad \text{at} \quad z = 0, l. \qquad \text{(A.2.2)}$$

Consider the behavior of x_j described by (A.2.1) and (A.2.2) about the uniform steady state x_{st}, the coordinates of which (ψ_{st}, ρ_{st}, $[X]_{st}$, e_{st}) were determined from the following equations: $Q_j = 0$, $j = 1, 2, 3, 4$.

Equations (A.2.1) linearized in the neighborhood of the steady state can be re-written in terms of small deviations $y_j = x_j - x_{st}$:

$$\frac{\partial y_j}{\partial t} = D_j \frac{\partial^2 y_j}{\partial z^2} + \sum_{n=1}^{4} m_{jn} y_n, \quad j = 1, 2, 3; \qquad \text{(A.2.3a)}$$

$$\frac{\partial y_4}{\partial t} = D_4 \frac{\partial^2 y_4}{\partial z^2} + D_4 N_e e_{st} \frac{\partial^2 y_1}{\partial z^2}. \qquad \text{(A.2.3b)}$$

In Eqs. (A.2.3), the second and the higher order terms were omitted, and the linearization coefficients were:

$$m_{jn} = \left.\frac{\partial Q_j}{\partial y_n}\right|_{y_n = 0}, \quad j = 1, 2, 3; \quad n = 1, 2, 3, 4.$$

From (2–4) and (5) the derivatives in the formulae of linearization coefficients were determined on the basis of the assumed models of the sources as follows:

$$m_{11} = \frac{\partial Q_1}{\partial \psi} = -\frac{1}{C_m}\left(\frac{\partial}{\partial \psi}(J_Y + J_X + J_p) + G_L\right);$$

$$m_{12} = \frac{\partial Q_1}{\partial \rho} = -\frac{J_X}{C_m \rho_{st}};$$

$$m_{13} = \frac{\partial Q_1}{\partial [X]_i} = -\frac{1}{C_m}\frac{\partial}{\partial [X]_i}(J_X + J_p); \quad m_{14} = 0;$$

$$m_{21} = \frac{\partial Q_2}{\partial \psi} = \frac{e_{st}\,\alpha\,\beta}{(\alpha+\beta)};$$

$$m_{22} = \frac{\partial Q_2}{\partial \rho} = -(\alpha+\beta);$$

$$m_{23} = 0; \quad m_{24} = \alpha;$$

$$m_{31} = \frac{\partial Q_3}{\partial \psi} = -\frac{\beta}{\chi F}\frac{\partial}{\partial \psi}(J_X + 3J_p);$$

$$m_{32} = \frac{\partial Q_3}{\partial \rho} = -\frac{\beta}{\chi F}\frac{\partial J_X}{\partial \rho};$$

$$m_{33} = \frac{\partial Q_3}{\partial [X]_i} = -\frac{\beta}{\chi F}\frac{\partial}{\partial [X]_i}(J_X + 3J_p) - P_X; \quad m_{34} = 0.$$

The boundary conditions (A.2.2) remained the same. We searched for a solution of the linearized problem in the form of $y_j = A_j \exp(\omega t + \mathrm{i}kz)$. The characteristic equation for the system (A.2.3) in the neighborhood of the steady state was:

(A.2.4)

$$Det \begin{vmatrix} m_{11}-\omega-D_1k^2 & m_{12} & m_{13} & 0 \\ m_{21} & m_{22}-\omega & 0 & m_{24} \\ m_{31} & m_{32} & m_{33}-\omega-D_3k^2 & 0 \\ -D_4\,N_e\,e_{st}\,k^2 & 0 & 0 & -\omega-D_4k^2 \end{vmatrix} = 0,$$

where k is the wave-number defining spatial period of the solution.

Values of ω defined the behavior of the system (its movement in the phase space) and the condition of stability about the steady state. According to the second Lapunov method (asymptotic stability theorem), the point model was stable in relation to small perturbations, if there was no roots with $Re(\omega) > 0$ of the point characteristic equation obtained from (A.2.3) with $D_j = 0$, $j = 1, 3, 4$ (Nicolis and Prigogine 1977). In this case the characteristic equation of the point system was:

$$Det\,|M - I\,\omega| = 0,$$

where M is the three-dimensional matrix of the elements m_{ij}, $i, j = 1, 2, 3$; and I is the unit matrix. According to the Routh-Hurwitz criterion (Korn and Korn 1968) the point system is stable when the following conditions held:

$$Tr(M) = m_{11} + m_{22} + m_{33} + m_{44} < 0, \qquad \text{(A.2.5a)}$$

$$Det(M) < 0, \qquad \text{(A.2.5b)}$$

$$-Tr(M)\,(A_{11} + A_{22} + A_{33}) + Det(M) > 0, \qquad \text{(A.2.5c)}$$

where

$$A_{11} = \begin{vmatrix} m_{22} & m_{23} \\ m_{32} & m_{33} \end{vmatrix}, \quad A_{22} = \begin{vmatrix} m_{11} & m_{13} \\ m_{31} & m_{33} \end{vmatrix}, \quad A_{33} = \begin{vmatrix} m_{11} & m_{12} \\ m_{21} & m_{22} \end{vmatrix}$$

are the minors of the elements m_{11}, m_{22} and m_{33}, respectively. These necessary and sufficient conditions defined the parametric domain within which the combined point equations had no infinitely increasing solutions. In this case the suggested model of sources was physically realizable.

We have determined the conditions when the original system (at $D_j \neq 0$) with physically realizable spatially distributed kinetics was unstable in relation to spatially nonuniform perturbations. If the solution of the spatially distributed system was unstable in the neighborhood of a singular point, then at least one value of ω existed with $Re(\omega) > 0$. If the characteristic equation had an even number of the roots with $Re(\omega) > 0$, then the instability was oscillatory and led to the occurrence of so-called dynamical *DSs* in the form of auto-oscillations (Kerner and Osipov 1990). The Turing instability leading to creation of steady *DSs* corresponded to an odd number of such roots.

From the Routh-Hurwitz criterion of stability of linear systems (Korn and Korn 1968) it followed that the necessary and sufficient condition for the existence of *DSs* was the negativity of free term of characteristic equation (A.2.4):

$$\Phi(k^2) = -D_e k^2 (A k^4 + B k^2 + C) < 0, \qquad \text{(A.2.6)}$$

where

$$A = D_\psi D_X m_{22},\ B = -(D_\psi A_{11} + D_X A_{33} + D_X e_{st} N_e m_{12} m_{24}),$$

and

$$C = e_{st} N_e m_{24} (m_{12} m_{33} - m_{13} m_{32}) + Det(M).$$

Thus, we have found the necessary and sufficient conditions of creation of *DSs* in the model under study.

References

Bacskai BJ, Wallen P, Lev-Ram V, Grillner S, Tsien RY (1995) Activity-related calcium dynamics in lamprey motoneurons as revealed by video-rate confocal microscopy. Neuron 14: 19–28

Becchetti A, Arcangeli A, Del-Bene MR, Olivotto M, Wanke E (1992) Intra- and extracellular surface charges near Ca^{2+} channels in neurons and neuroblastoma cells. Biophys J 63: 954–965

Bedlack RSJ, Wei MD, Fox SH, Gross E, Loew LM (1994) Distinct electric potentials in soma and neurite membranes. Neuron 13: 1187–1193

Cai M, Jordan PC (1990) How does vestibule surface charge affect ion conduction and toxin binding in a sodium channel? Biophys J 57: 883–891

Chad JE, Eckert R (1984) Calcium domains associated with individual channels can account for anomalous voltage relations of Ca-dependent responses. Biophys J 45: 993–999

Cukierman S (1991) Asymmetric electrostatic effects on the gating of rat brain sodium channels in planar lipid membranes. Biophys J 60: 845–855

Eun-hye Joe, Angelides KJ (1993) Clustering and mobility of voltage-dependent sodium channels during myelination. J Neuroscience 13: 2993–3005

Fromherz P, Zimmermann W (1995) Stable spatially periodic patterns of ion channels in biomembranes. Phys Rev E 51: R1659–R1662

Garrahan PJ, Garay RP (1974) A kinetic study of the Na-pump in red cells: its relevance to the mechanism of active transport. Ann NY Acad Sci 242: 445–458

Gogan P, Schmiedel-Jakob I, Chitti Y, Tyč-Dumont S (1995) Fluorescence imaging of local membrane electric fields during the excitation of single neurons in culture. Biophys J 69: 299–310

Goldman DE (1943) Potential, impedance, and rectifications in membranes. J Gen Physiol 27: 36–60

Henzi V, MacDermott AB (1992) Characteristics and function of Ca^{2+} and inositol 1,4,5-trisphosphate-releasable stores of Ca^{2+} in neurons. Neuroscience 46: 251–273

Hille B (1992) Ionic channels of excitable membranes. Sinauer Associates, Inc, Sunderland, Mass
Jack JJB, Noble D, Tsien RW (1983) Electric current flow in excitable cells. Oxford University Press, London
Jaffe LF (1977) Electrophoresis along cell membranes. Nature 265: 600 – 602
Jaffe DB, Johnston D, Lasser-Ross N, Lisman JE, Miyakawa H, Ross WN (1992) The spread of Na spikes determines the pattern of dendritic Ca entry into hippocampal neurons. Nature 357: 244 – 246
Johnston D, Magee JC, Colbert CM, Christie BR (1996) Active properties of neuronal dendrites. Annu Rev Neurosci 19: 165 – 186
Kerner B, Osipov V (1990) Self-organization in active distributed media. Uspekhi Fizicheskikh Nauk (USSR) 160: 1 – 73
Korn GA, Korn TM (1968) Mathematical handbook. McGraw-Hill, New York
Kotyk A, Janacek K, Koryta J (1988) Biophysical chemistry of membrane functions. Wiley, Chichester
Kurata K, Kisimoto K, Yanagida E (1989) The asymptotic transectional/circumferential homogeneity of the solutions of reaction-diffusion systems in/on cylinder-like domains. J Math Biol 27: 485 – 490
Lankaster B, Zuker R (1994) Photolytic manipulation of Ca^{2+} and the time course of slow, Ca^{2+}-activated K^+ current in rat hippocampal neurones. J Physiol 475: 229 – 239
Lav-Ram V, Miyakawa H, Lasser-Ross N, Ross W (1992) Calcium transients in cerebellar Purkinje neurons evoked by intracellular stimulation. J Neurophysiol 68: 1167 – 1177
Lemieux DR, Roberge F, Savard P (1990) A model study of the contribution of active Na-K transport to membrane repolarization in cardiac cells. J Theor Biol 142: 1 – 33
Llinas RR (1988) The intrinsic electrophysiological properties of mammalian neurons: insight into central nervous system function. Science 242: 1654 – 1664
Magee JC, Johnston D (1995) Characterization of single voltage-gated Na^+ and Ca^{2+} channels in apical dendrites of rat CA 1 pyramidal neurons. J Physiol 481: 67 – 90
Murray JD (1989) Mathematical biology, 2nd edn. Springer, Berlin Heidelberg New York
Nicolis G, Prigogine I (1977) Self-organization in nonequilibrium systems. Wiley, New York
Peaceman DW, Rachford HH (1955) The numerical solution of parabolic and elliptic differential equations. J Soc Indust Appl Math 3: 28 – 41
Peters R (1981) Translational diffusion in the plasma membrane of single cells as studied by fluorescence microphotolysis. Cell Biol Int Rep 5: 733 – 782
Pongracz F, Firestein S, Shepherd GM (1991) Electrotonic structure of olfactory sensory neurons analyzed by intracellular and whole cell patch techniques. J Neurophysiology 65: 747 – 754
Qian N, Sejnowski TJ (1989) An electro-diffusion model for computing membrane potentials and ionic concentrations in branching dendrites, spines and axons. Biol Cybern 62: 1 – 15
Rall W (1977) Core conductor theory and cable properties of neurons. The nervous system, Sect 1. Cellular biology of neurons. In: Kandell E-R et al. (eds) Handbook of physiology. Am Physiol Soc, Bethesda, pp 39 – 98
Ryan TA, Myers J, Holowka D, Baird B, Webb WW (1988) Molecular crowding on the cell surface. Science 239: 61 – 64
Savtchenko LP, Korogod SM (1994) Domains of calcium channels as dissipative structures in a simulated neuron. Neurophysiology 26: 99 – 107
Shaw PJ, Ince PG, Matthews JN, Johnson M, Candy JM (1994) N-methyl-D-aspartate (NMDA) receptors in the spinal cord and motor cortex in motor neuron disease: a quantitative autoradiographic study using MK-801. Brain Res 637: 297 – 302
Sherman A, Keizer J, Rinzel J (1990) Domain model for Ca^{2+}-inactivation of Ca^{2+} channels at low channel density. Biophys J 58: 985 – 995
Singer SJ (1975) The molecular organization of membranes. Annu Rev Biochem 244: 731 – 739
Spruston N, Schiller Y, Stewart G, Sakmann B (1995) Activity-dependent action potential invasion and calcium influx into hippocampal CA 1 dendrites. Science 268: 297 – 300
Stuart GJ, Dodt HU, Sakmann B (1993) Patch-clamp recordings from the somata and dendrites of neurones in brain slices using infrared video microscopy. Pfluegers Arch 423: 511 – 518
Tsien RW, Tsien RY (1990) Calcium channels, stores and oscillations. Annu Rev Cell Biol 6: 715 – 760
Turing AM (1952) The chemical basis of morphogenesis. Phil Trans Roy Soc Lond B237: 37 – 72
Yuste R, Tank DW (1996) Dendritic integration in mammalian neurons, a century after Cajal. Neuron 16: 701 – 716